ARTICLE OPEN

Check for updates

Transcriptional changes in specific subsets of *Drosophila* neurons following inhibition of the serotonin transporter

Shivan L. Bonanno[1] and David E. Krantz[1]✉

The transcriptional effects of SSRIs and other serotonergic drugs remain unclear, in part due to the heterogeneity of postsynaptic cells, which may respond differently to changes in serotonergic signaling. Relatively simple model systems such as *Drosophila* afford more tractable microcircuits in which to investigate these changes in specific cell types. Here, we focus on the mushroom body, an insect brain structure heavily innervated by serotonin and comprised of multiple different but related subtypes of Kenyon cells. We use fluorescence-activated cell sorting of Kenyon cells, followed by either bulk or single-cell RNA sequencing to explore the transcriptomic response of these cells to SERT inhibition. We compared the effects of two different *Drosophila* Serotonin Transporter (*dSERT)* mutant alleles as well as feeding the SSRI citalopram to adult flies. We find that the genetic architecture associated with one of the mutants contributed to significant artefactual changes in expression. Comparison of differential expression caused by loss of SERT during development versus aged, adult flies, suggests that changes in serotonergic signaling may have relatively stronger effects during development, consistent with behavioral studies in mice. Overall, our experiments revealed limited transcriptomic changes in Kenyon cells, but suggest that different subtypes may respond differently to SERT loss-of-function. Further work exploring the effects of SERT loss-of-function in other circuits may be used help to elucidate how SSRIs differentially affect a variety of different neuronal subtypes both during development and in adults.

Translational Psychiatry (2023)13:226 ; https://doi.org/10.1038/s41398-023-02521-3

INTRODUCTION

Though serotonergic neurons comprise only ~1/200,000 neurons in humans, they project to and influence nearly every region of the mammalian brain [1, 2], and represent a commonly targeted neurotransmitter system in the treatment of depression [3–6]. The predominant method by which serotonin is cleared from the extracellular space is through reuptake into the presynaptic cell by the plasma membrane serotonin transporter (SERT) [7–10]. SERT is the target of selective serotonin reuptake inhibitors (SSRIs), which inhibit its activity and thus prolong the availability of extracellular serotonin to bind and activate serotonin receptors (5-HTRs). Widespread prescription of these drugs has motivated many studies of their long-term effects utilizing peripheral samples [11–13] or highly heterogeneous brain tissue [14, 15]. However, a deeper understanding of serotonergic circuits and their responses to therapeutic interventions remains elusive due in part to the heterogeneity of serotonergic neurons themselves and the cells that they innervate. Such cellular diversity has been highlighted recently in mammals [1, 16, 17], and a few studies have analyzed gene expression in specific populations of cells postsynaptic to serotonergic neurons [18, 19]. Several reports have investigated changes in ribosome-loaded RNA in a particular cell type after environmental/behavioral perturbations and/or SSRI administration [20, 21]. Another recent study has generated multi-omic datasets on fluoxetine vs. sham-treated mice across multiple brain regions, including two datasets utilizing single-cell RNA-seq (scRNA-seq) to analyze specific hippocampal cell types [14]. The complexity of these findings suggests that further, detailed analysis of the response that occurs in different subtypes of neurons will be necessary to fully understand the molecular effects of SERT inhibition.

Similar to the mammalian CNS, the *Drosophila* brain is innervated by relatively few (~90) broadly projecting serotonergic neurons [22–24]. Due to its relative simplicity, it is much easier to identify structures and circuits in the *Drosophila* brain that are innervated by one or a few, particular serotonergic neurons. This, coupled with the genetic tools available in flies, affords a technically tractable platform for the molecular interrogation of serotonergic circuits and in particular, specific subsets of post-synaptic neurons that receive serotonergic inputs.

The mushroom bodies (MBs) are structures in the central brain of *Drosophila* and other insects required for learning as well as other behaviors [25]. They are densely innervated by a small number of serotonergic cells [26–31] and are comprised of three major cell subtypes of Kenyon cells (KCs) including α/β, α′/β′, and γ KCs, which can be further subdivided based on morphology, birth order, and gene expression [32, 33]. The three major KC subtypes are known to differ in 5-HTR expression profiles [33, 34], with 5-HT1A enriched in $KC_{\alpha/\beta}$ and 5-HT1B in KC_{γ} proposed to regulate different behavioral outputs [35–37].

We have employed bulk RNA-seq as well as scRNA-seq following the isolation of KCs and identified a small number of genes that are differentially expressed in the MBs following inhibition of SERT activity. Our results also highlight several

[1]Department of Psychiatry and Biobehavioral Sciences, David Geffen School of Medicine, University of California, Los Angeles, CA 90095, USA. ✉email: dkrantz@ucla.edu

Received: 24 February 2023 Revised: 6 June 2023 Accepted: 13 June 2023
Published online: 24 June 2023

technical considerations relevant to further transcriptional studies of serotonergic circuits.

METHODS

Fly husbandry

Flies were maintained on a standard cornmeal and molasses-based agar media with a 12:12 h light/dark cycle at room temperature (22–25 °C).

For experiments involving drug-induced SERT blockade, female flies were sorted on the day of eclosion and maintained on 1% agar + 5% sucrose + 1% blue food dye, with or without the addition of 3 mM citalopram (Sigma, St. Louis, MO, USA, PHR1640), for 4–6 days before dissection.

Generation of *dSERT^{TMKO}* null allele

The *dSERT* genomic locus was analyzed and the portion corresponding to most of the first and second transmembrane domains was identified (~2.6 kb) for deletion, reasoning that excision of these crucial regions along with a simultaneous frameshift mutation would result in a null allele. The donor vector for the *dSERT^{TMKO}* allele was then generated according to a previously described protocol [38]. Briefly, ~1 kb homology arms flanking the 5′ and 3′ end of the region to be excised were obtained by PCR. All primers are listed below and written 5′–3′. 5′ arm: Fwd: ATATAGAATTCC-CACACAGACACACACATGCGTC and Rev: TATATGCTAGCGGATGTGACGGC-CATTCGCAGC (underlined is mutated PAM site). 3′ arm: Fwd: ATATACTGCAGGAGCGGAATCTACAAAACGTGGCC and Rev: TATATCTC-GAGGGTCTCGAACCGCAGAATGATTCC. The 5′ and 3′ homology arms were then cloned sequentially into pHD-DsRed (DGRC plasmid 1360) using EcoRI/NheI and PstI/XhoI, respectively. Two sgRNA sequences, one targeting the 5′ end and one targeting the 3′ end of the portion to be deleted, were identified using the UCSC genome browser and integrated quality assessment tools [39, 40]. DNA oligos corresponding to these sequences (sg1: Fwd: TTCGGCTGCGAATGGCCGTCACAT, Rev: AAACATGT-GACGGCCATTCGCAGC, sg2: Fwd: TTCGAAAGTTTATCTGTGCCGCTC, Rev: AAACGAGCGGCACAGATAAACTTT) were phosphorylated in vitro and cloned into pU6-BbsI-gRNA (Addgene 45946) [41]. The donor vector and both sgRNA plasmids were sent to Best Gene, Inc (Chino Hills, CA) for injection into *Drosophila* embryos from strains expressing Cas9 in the germline (Vas-Cas9, BDSC:51324). Transformants were identified using 3xP3-DsRed and crossed to balancers to create stable lines. These lines were then back-crossed to *w^{1118}* for 6 generations to remove off-target mutations that may have arisen during injection, and to render the rest of the second chromosome more similar to the *w^{1118}* genetic background to which it was to be compared in sequencing experiments. The final, outcrossed allele was then crossed to CyO,Cre [42], to excise the floxed 3xP3-DsRed marker, and re-crossed to balancers to obtain the *dSERT^{TMKO}* allele used in this study.

Additional fly lines/alleles used

The following fly lines were used in this study are as follows, with stock numbers for lines obtained from the Bloomington *Drosophila* Stock Center (BDSC, Bloomington. IN, USA) listed in parentheses: *w^{1118}* (BDSC:5909), *Mef2-gal4* (BDSC:50742), *UAS-nls.GFP* (BDSC:4776), *CyO,Cre* (BDSC:1092), *dSERT^{4}* (gift from H. Schölz), *dSERT^{16}* (gift from H. Schölz), *dSERT^{TMKO}* (created in this work), DGRP-21 (BDSC:28122), DGRP-129 (BDSC:28141), DGRP-235 (BDSC:28275), DGRP-304 (BDSC:25177), DGRP-320 (BDSC:29654), DGRP-324 (BDSC:25182), DGRP-354 (BDSC:55020), DGRP-382 (BDSC:28189), DGRP-383 (BDSC:28190), DGRP-395 (BDSC:55022), DGRP-406 (BDSC:29657), DGRP-437 (BDSC:25194), DGRP-461 (BDSC:28200), and DGRP-819 (BDSC:28242).

FACS and RNA-seq library preparation

Fly lines were constructed as described, bearing *Mef2(P247)-gal4* driving *UAS-nls.GFP* to label Kenyon cell (KC) nuclei. Brains were dissected on the day of eclosion (day 0, Figs. 1–3), or day 4–6 (Figs. 4, 5) and the optic lobes removed. Central brains were pooled and dissociated according to previously published methods [43]. The dissociated brain cells were separated by fluorescence-activated cell sorting (FACS) into GFP-positive and GFP-negative isolates using a BD FACS Aria II high-speed cell sorter at the UCLA Jonsson Comprehensive Cancer Center (JCCC) and Center for AIDS Research Flow Cytometry Core Facility [26–31].

Bulk RNA-seq

For each bulk RNA-seq replicate, 18–40 brains were dissected per genotype. Cells were collected directly off FACS (5900–10,400 GFP^{+} cells per replicate) and lysed immediately in Buffer RLT (Qiagen #79216, MD, USA). RNA was purified using a commercial column (RNeasy kit, Qiagen #74034). RNA was stored at −80 °C until 5 replicates per condition were collected. Libraries for all 10 samples were prepared simultaneously according to the SMART-seq v2 Ultra Low-input RNA sequencing kit with Nextera XT (Takara Bio, MD, USA, v4 #634893), using a protocol adapted from [44–46] and available upon request. Libraries were sequenced with spike-in Phi-X at the UCLA BSRC High Throughput Sequencing Core (https://stemcell.ucla.edu/high-throughput-sequencing) on an Illumina NovaSeq SP 2 × 50 bp. After demultiplexing, 24–88 million reads per sample were retained. Quality control was performed using base metrics and nucleotide composition of raw reads. Alignment to the *Drosophila melanogaster* genome (BDGP6) was performed using the STAR spliced read aligner [47] with default parameters. Only uniquely mapped reads were used for subsequent analyses. PCA analysis showed that one pair of samples had modestly increased technical variability, and was removed from subsequent analyses. Differential expression was calculated between mutant and WT samples using DESeq2 [48].

scRNA-seq

For each single-cell RNA-seq experiment, 7–12 brains were dissected per genotype, and the genotypes were pooled for subsequent processing. GFP^{+} cells representing all of the pooled samples were isolated via FACS (6500–10,000 per experiment), collected in Schneider's media containing BSA, and transported immediately to the UCLA Technology Center for Genomics and Bioinformatics (TCGB) Core Facility (https://www.uclahealth.org/pathology/tcgb) for sample processing using the *10x Genomics* 3′ GEX v3 platform. For experiments in Fig. 2 (*dSERT^{16}*, day 0) and Fig. 3 (*dSERT^{TMKO}*, day 0), all cells from each experiment were loaded on an individual chip from *10x Genomics*, thus reducing variability between technical replicates caused by differences in sample preparation seen in most other RNA-seq methods. All of the cells from experiments in Fig. 4 (*dSERT^{TMKO}*, days 4–6) and Fig. 5 (CIT, days 4–6) were combined and loaded onto a single *10x* chip. For all *10x* chips, the maximum sample volume was loaded, targeting an upper limit of ~10,000 cells. cDNA and libraries were prepared and checked for size distribution by ScreenTape analysis (Agilent Technologies, Carpinteria, CA, USA). Libraries were sequenced on an *Illumina* NovaSeq SP 2x50bp. Raw sequencing reads were processed using Cell Ranger (7.0.0) with default parameters. The reference genome and gene annotations were obtained from FlyBase (6.29). Processed single-cell transcriptomes were demultiplexed based on parental genotypes using demuxlet (version 2, https://github.com/statgen/popscle) [49]. In total, genotypes of 14 DGRP strains were used for demultiplexing: DGRP-21, DGRP-129, DGRP-235, DGRP-304, DGRP-320, DGRP-324, DGRP-354, DGRP-382, DGRP-384, DGRP-395, DGRP-406, DGRP-437, DGRP-461, DGRP-819 (http://dgrp2.gnets.ncsu.edu) [50]. The genomic coordinates of variants were transformed from the dm3 to the dm6 version of the Drosophila reference genome using Crossmap [51]. The following criteria were used to filter variants used for the analysis: (1) only variants residing on chromosome 3; (2) only biallelic single-nucleotide polymorphisms (SNPs) that were called in all analyzed DGRP strains with a maximum non-reference allele count of 2 (i.e. SNPs detected in only one of the strains); (3) the non-DGRP chromosome 3 was analyzed for SNPs that could be shared with DGRP strains, and those variants were removed from the analysis. BAM files from Cell Ranger were used to generate read pileups and to estimate allelic frequencies in our datasets. Alleles detected with high-frequency (i.e. half of the total reads deriving from the third chromosome) are expected to originate from the common non-DGRP chromosome. Only SNPs with minimum coverage of 5 reads and minor-allele frequencies <0.2 were kept for the analysis. The processing of the VCF file was performed using VCFtools [52], and SAMtools [53]. The final set included 93,084 SNPs, which were transformed into heterozygous variants for the demultiplexing of F1 samples (i.e. alleles were modified from 1/1 to 1/0). The same VCF file was used for demultiplexing of all experiments. Data from all experiments were combined and demultiplexed simultaneously. During demultiplexing, we confirmed that cells were not spuriously assigned to DGRP genotypes that were not present in a particular experiment. Raw sequencing reads and the VCF file for demultiplexing are available at the NCBI GEO repository (GSE227935).

Single-cell data analysis was performed using Seurat (v4.1.1) [54, 55]. Single-cell transcriptomes were filtered using the following criteria: (1)

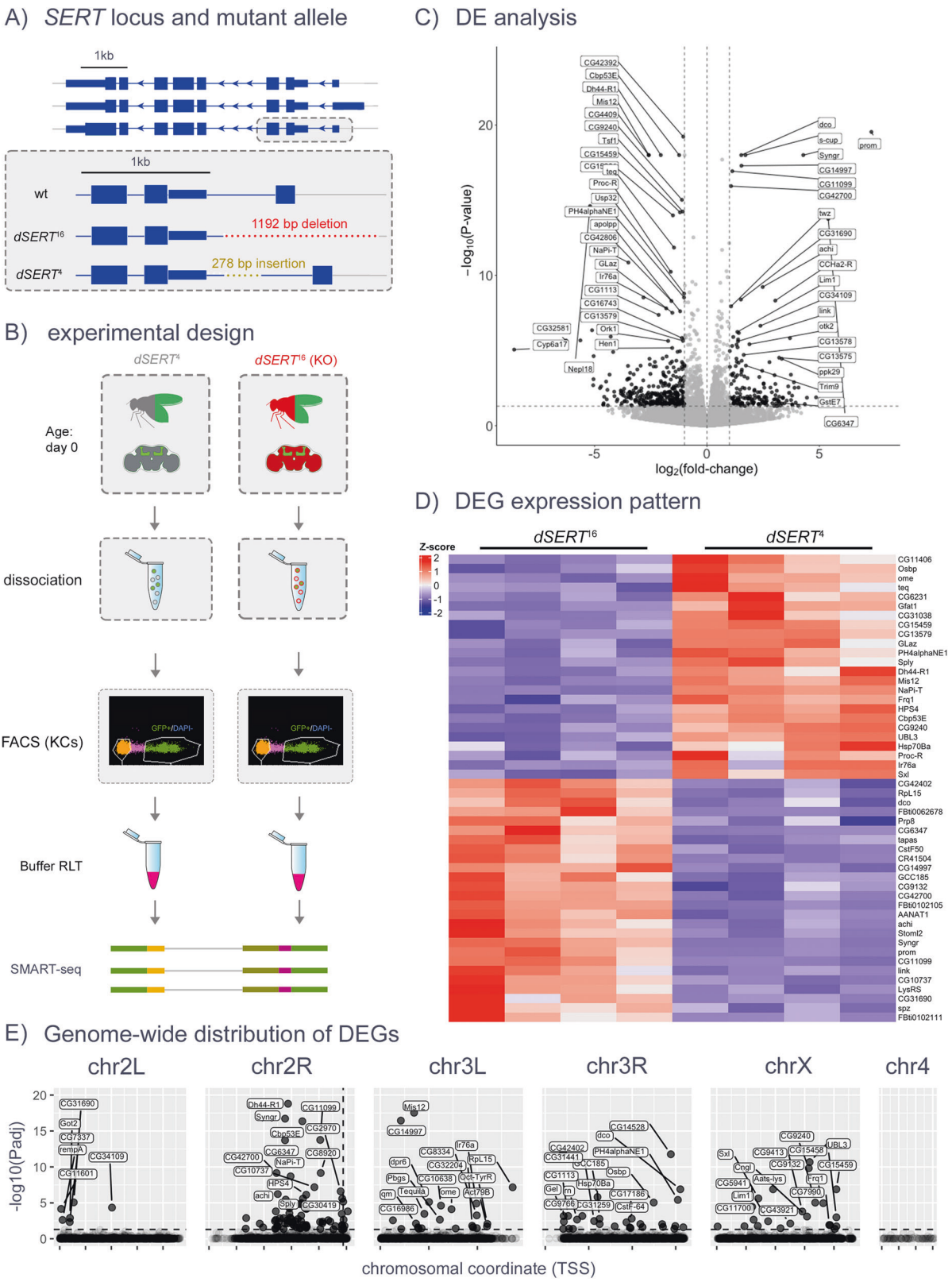

transcript count ≥1000; (2) a maximum percentage of mitochondrial transcripts ≤ 20%; (3) we also removed cells that were classified by demuxlet as "doublets/ambiguous", and cells that were assigned to the genotypes that were not used in the given experiment.

Filtered datasets from all three experiments were analyzed together. First, we integrated all datasets using Seurat V3 workflow with default parameters [54]. The integrated dataset was used for unsupervised clustering using the standard Seurat workflow (principal components: 1:10, resolution: 0.3). This analysis revealed 13 clusters, of which six expressed markers of Kenyon cells (Supplementary Fig. S1A, B). We then removed non-KC clusters and re-ran integration and clustering steps (principal components: 1:10, resolution: 0.1), which yielded 8

Fig. 1 Bulk RNA-seq of KCs, in immediately eclosed (day 0) flies. A The *Drosophila dSERT* locus encodes three transcripts (top panel). The *dSERT*^{16} mutant bears a 1.1 kb deletion at the 5′ end that includes a non-coding exon and upstream regulatory DNA. The *dSERT*^{4} genetic background-matched control contains a 278 bp deletion but does not significantly alter protein expression or behavior compared to WT [67]. **B** Sample preparation for bulk sequencing. Flies contained the *Mef2(P247)-gal4* driver and *UAS-nls.GFP* marker for expression in KCs, and were homozygous for either *dSERT*^{16} (mutant) or *dSERT*^{4} (control) on the second chromosome. Flies were dissected and pooled by genotype, then dissociated and FACS-sorted in parallel to select for GFP-labeled KCs, followed by isolation of RNA for bulk RNA-seq (SMART-seq). **C** Volcano plot showing differential expression between *dSERT*^{16} and *dSERT*^{4} groups. DE genes include those encoding the transcription factors *Lim1* and *Achi*, the channels *Ork1* and *Ppk29*, the GPCRs *Dh44-R1, Proc-R, CCHa2-R*, and *Ir76a*, the calcium-binding protein *Cbp53E*, and genes implicated in neuronal development (*Trim9, Mis12*). **D** The top 50 DE genes are shown as a *z*-score heatmap. **E** DEGs plotted by chromosomal coordinates of genomic locus, with inverse $\log_{10}(p_{adj})$ on the *y*-axis. The horizontal dashed line represents $p_{ad} \leq 0.05$ cutoff. A large number of DE genes localize to the same chromosomal arm (chr2R) as *dSERT* (vertical dashed line).

transcriptionally distinct populations of KCs. These clusters were annotated based on known marker genes of KC subtypes (Supplementary Fig. S1B, C). Three small clusters were present only in one of three experiments and were excluded from further analysis (KC_G3, KC_G4, and KC_AB3).

Differential gene expression analysis was performed for each KC cluster and each experiment separately using the "pseudobulk" approach [56] as follows: read counts from single-cell transcriptomes were first aggregated at the level of biological replicates (i.e. DGRP strains, see above for details). Differential expression analysis was then performed between control and mutant/drug samples using DESeq2 [48]. Differentially expressed genes were identified at adjusted *p*-value (p_{adj}) ≤ 0.05 and fold-change ≥ 1.5.

Data in all figures were processed and plotted using the following R packages: ggplot2 [57], tidyverse [58], ggrepel [59], patchwork [60], nVennR [61], Libra [62], DESeq2 [48], edgeR [63, 64], Limma [65], and Seurat [54, 55, 66].

RESULTS

To achieve a complete loss of dSERT activity we focused our initial experiments on *dSERT* mutants rather than drug-induced blockade. We used previously described flies homozygous for a *P*-element-excision-derived mutant allele (*dSERT*^{16}) or a genetically matched control (*dSERT*^{4}) with wild-type (WT) dSERT expression [67] (Fig. 1A) and *Mef2(P247)-gal4* [68] driving nuclear-localized GFP to label Kenyon cells. This driver captures most of the KCs across all 3 subtypes α/β, α′/β′, and γ [69] but is enriched for α/β and γ relative to α′/β′. We collected female flies on the day of eclosion and dissected brains from *dSERT*^{4} *and dSERT*^{16}. KCs from each genotype were dissociated in parallel and isolated via FACS using the GFP marker (Fig. 1B). Five replicates per genotype were obtained and bulk RNA-seq libraries (SMART-seq) were prepared for all samples and sequenced together. PCA (data not shown) revealed two samples (one of each genotype) with increased technical variability; these were removed from subsequent analyses.

Differentially expressed genes (DEGs) between *dSERT*^{16} and *dSERT*^{4} samples were identified using DESeq2 [48] and revealed 44 upregulated and 54 downregulated ($p_{adj} < 0.05$) (Fig. 1C, D and Supplementary Table T1). These include DEGs with functions that could represent homeostatic adjustments to perturbations in serotonergic signaling during development, such as transcription factors (*Lim1*, *Achi*), proteins involved in neuronal maturation and development (*Trim9*, *Mis12*) [70, 71], a *Drosophila* ortholog of calbindin (*Cbp53E*), ion channels (*Ork1*, *Ppk29*), and several GPCRs (*Dh44-R1*, *Proc-R*, *CCHa2-R*, *Ir76a*) (Fig. 1C, D and Supplementary Table T1). When genes were plotted by chromosomal position, however, there was a striking concentration of DEGs on the same arm of the 2nd chromosome (chr2R) as the *dSERT*^{16} DNA lesion (Fig. 1E). *Drosophila* has only 3 chromosomes that house most of their genome, and some of these observations may represent true findings. However, the buildup on chr2R suggests that at least some of the observations may derive from the disruption of genomic DNA rather than changes in serotonergic signaling.

Though SMART-seq libraries feature increased sensitivity to lowly expressed transcripts, they necessitate the pooling of RNA from all cell types within the collected population and may result in a washout of cell-type-specific changes. To investigate the transcriptomics of each KC subtype independently, we followed a recent single-cell RNA-seq strategy in which all samples and replicates are pooled and processed together [43, 49]. We generated *dSERT*^{16} and *dSERT*^{4} fly lines with GFP expressed in KCs as above, but included an additional element unique to each biological replicate: a 3rd chromosome derived from independent WT strains available from the *Drosophila* Genetics Research Panel (DGRP)[50]. Because transcripts derived from DGRP chromosomes bear SNPs, single cells can be bio-informatically traced to genotype-of-origin post-hoc (Fig. 2A). This allowed us to pool all replicates of both control and mutant samples for dissociation, FACS, library prep, and sequencing, thereby minimizing long-standing issues of technical variability between individual replicates that contribute to bias in RNA-seq data. Dimensionality reduction (Supplementary Fig. S1) resulted in robust clusters for two sub-populations for $KC_{\alpha/\beta}$ (KC_AB1, KC_AB2), two for KC_{γ} (KC_G1, KC_G2), and one for $KC_{\alpha'/\beta'}$ (KC_ABp1) (Fig. 2B). Running pseudobulk differential expression between mutant and control cells collapsed by cell-type revealed 33 significant changes. Some changes were cell-type specific (e.g. *SK* in KC_G1 and *CG31690* in KC_AB1), and many were observed in multiple cell-types (e.g. *prom*, *Cbp53E*, *CG42392*, *Pgant9*) (Fig. 2C, D and Supplementary Table T2). For those DEGs that were identified as cell-type specific such as *SK*, we detected robust transcript expression in most of the clusters, lending credence to the hypothesis that the DE observed is in fact specific to a particular cell-type (Supplementary Fig. S2). When visualized in pseudo-Manhattan plots (Fig. 2E), however, the bias of DEGs to chr2R was even more pronounced than for SMART-seq (Fig. 1E), highlighting their possible artefactual provenance. The DEGs on chr2R appear to lie in two positional "columns"—one ~7.5 Mb away from *dSERT*, and one that is immediately adjacent to the *dSERT*^{16} deletion. One of the DEGs immediately adjacent to the deletion is an eye-specific gene, *prom*, that is not expressed in WT KCs. By extension, we concluded that the upregulation of the *prom* transcript in d*SERT*^{16} is likely to represent an artifact caused by the deletion of regulatory DNA adjacent to *dSERT* and *prom*.

To explore the possibility that more precise mutations in *dSERT* might be less disruptive and generate fewer artefactual hits, we generated a new mutant allele using CRISPR [38] to precisely excise ~2.6 kb DNA coding for most of the first and second transmembrane domains and simultaneously induce a frameshift in the CDS. We reasoned that even if the resultant mRNA could code for a partial dSERT protein, it would be topologically inverted in the plasma membrane and thus represents a null allele (Fig. 3A). Fly lines bearing the deletion, termed *dSERT*^{TMKO}, were outcrossed six times to *w*^{1118}. The presence of the deletion was confirmed by PCR-sanger sequencing, and behaviorally in that this line phenocopies the sleep deficit found in *dSERT*^{16} (data not shown). We then built fly lines as in the previous experiment, using the new *dSERT*^{TMKO} allele and second chromosomes derived from *w*^{1118} as controls, in place of *dSERT*^{16} and *dSERT*^{4}, respectively. Sample prep, scRNA-seq, and data processing (Fig. 3B) were performed using the same pipeline as for the previous

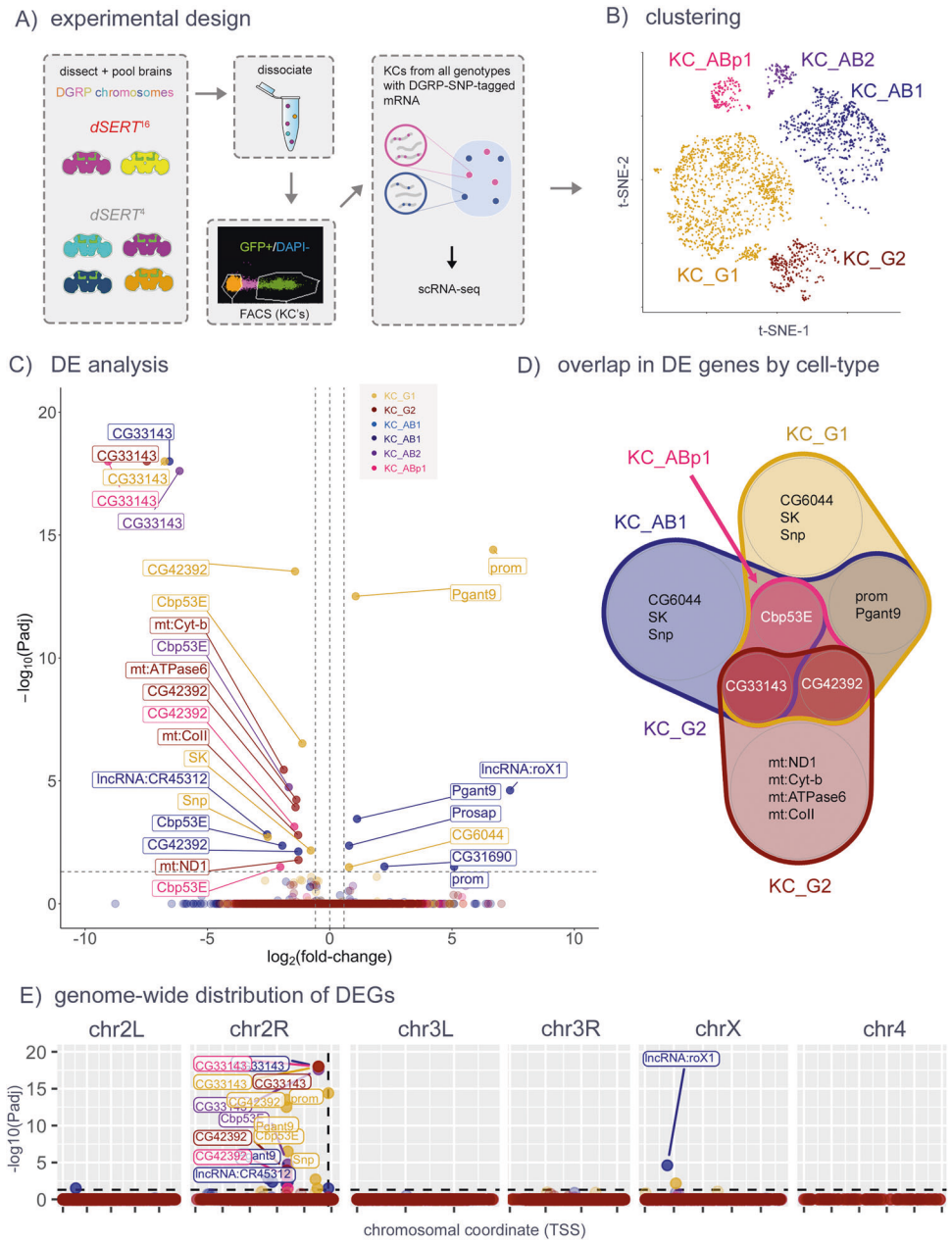

Fig. 2 scRNA-seq of KCs from d*SERT*^{16} and d*SERT*^{4} flies, in immediately eclosed (day 0) flies. A Flies used for scRNA-seq contained one of six unique third chromosomes derived from different DGRP wild-type lines, as well as the markers and *dSERT* alleles used for bulk seq. Two and four different DGRP lines per group (*dSERT*^{16} or *dSERT*^{4}, respectively) were created and served as biological replicates. Brains from all lines were dissected, pooled, and dissociated together, then FACS-sorted to select KCs used for scRNA-seq. **B** t-SNE dimensional reduction showing the distribution of cells in this dataset among transcriptionally-defined clusters (see the "Methods" section) representing KC_g cells (KC_G1, KC_G2), $KC_{a/b}$ (KC_AB1, KC_AB2), and $KC_{a'/b'}$ (KC_ABp1). **C** Volcano plot from "pseudobulk" analysis (by cluster) of DEGs between *dSERT*^{16} and *dSERT*^{4}. Observations are color-coded (as in **B**) by the KC type in which they were identified. **D** Venn diagram showing the overlap of DEGs identified in the major cell clusters. *Cbp53E*, *CG42392*, and *CG33143* were identified as DE in multiple cell types. **E** DEGs are plotted by chromosomal locus as in Fig. 1E. A skewed localization of DEGs to chr2R is notable.

experiment. Again, relatively few (13) DE observations were made between mutant and WT cells (Fig. 3C, Supplementary Table T3). However, in this dataset there is no pronounced enrichment of DEGs on chr2R (Fig. 3F). Importantly, some of the DEGs on chr2R in the previous (*dSERT*^{16}) dataset, including those immediately adjacent to *dSERT*, such as *prom*, are absent from this *dSERT*^{TMKO} dataset (Supplementary Fig. S2B). Some genes DE in this experiment were not detected in the previous dataset, such as *LysRS* in multiple cell types and *dpr1* and *mamo* in KC_ABp1 and KC_G2, respectively.

While it is known that KCs undergo extensive remodeling during pupation [72–76], most of the literature establishing the importance of serotonergic signaling onto them concerns behaviors such as sleep and memory, which are not utilized during pupation. We thus hypothesized that some of the transcriptional changes in response to *dSERT* LOF may not accumulate until the circuit undergoes perturbed activity in the adult fly brain. To assess transcriptional changes that may accumulate after eclosion, we repeated the *dSERT*^{TMKO} scRNA-seq in 4–6 day-old adult flies (Fig. 4A). This experiment yielded a

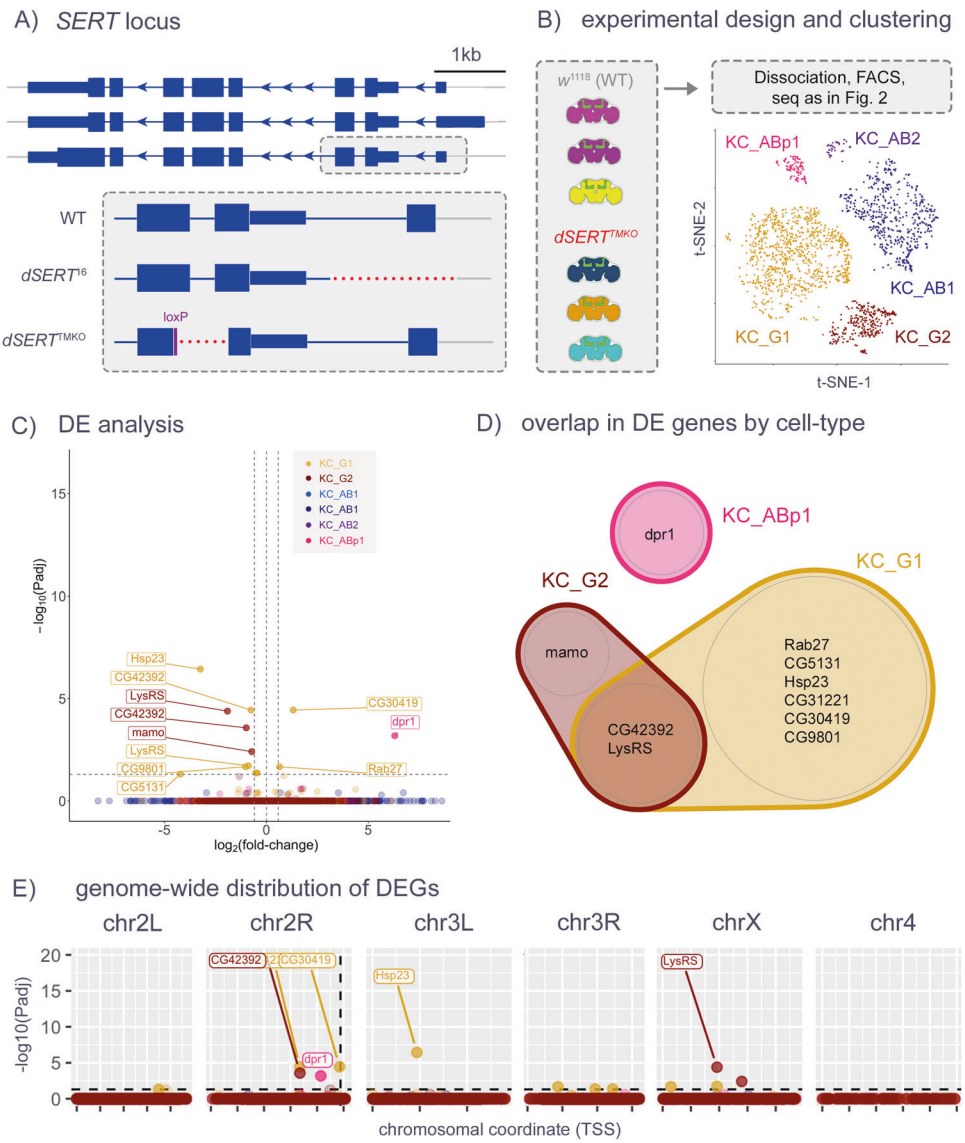

Fig. 3 d*SERT*^{TMKO} scRNA-seq, in immediately eclosed (day 0) flies. A Cartoon depicts the independently derived *dSERT*^{TMKO} deletion compared to *dSERT*^{16}. **B** Flies used for this scRNA-seq experiment were homozygous for *dSERT*^{TMKO} or a WT d*SERT* allele derived from *w*^{1118} and expressed with the same transgenes for isolation of KC cells as in Figs. 1 and 2. Each fly was marked by a different DGRP 3rd chromosome variant, and t-SNE plot shows the color-coded distribution of cells by KC cell type as in Fig. 2. **C** Volcano plot as in Fig. 2C from "pseudobulk" analysis (by cluster) of DEGs between mutant and control. Observations are color-coded (as in **B**) by the KC type in which they were identified. **D** Venn diagram showing overlap of DEGs identified in the major cell clusters. *CG42392* and *LysRS* were identified as DE in both KC_G1 and KC_G2. **E** DEGs are plotted by chromosomal position as in Fig. 2F. In contrast to Fig. 2, observations are not concentrated on chr2R.

lower cell number per cluster (Supplementary Fig. S1F) than those using freshly eclosed adults, limiting statistical power in calling DE. Nonetheless, we observed a small number (15) of DEGs between d*SERT*^{TMKO} mutant and WT cells (Fig. 4C, D and Supplementary Table T4). Interestingly, some genes (e.g. *LysRS*) were shared with the previous (day 0) dataset, while *Cbp53E*, a gene identified in the *dSERT*^{16} day 0 dataset but not found in the *dSERT*^{TMKO} day 0, reappeared in this *dSERT*^{TMKO} day 4–6 dataset.

The use of constitutive *dSERT* deletion mutants ensures complete and specific SERT LOF, but it is not possible to distinguish between developmental and adult effects. As a first step to study the effects of long-term SERT blockade in circuits that develop normally, we fed adult flies 3 mM citalopram (CIT) to pharmacologically inhibit SERT, a concentration that phenocopies the effect of the *dSERT*^{16} allele on sleep behavior [67]. After feeding WT flies either CIT or vehicle (VEH) from eclosion for 4–6 days (Fig. 5A), we again isolated GFP-tagged KCs and used single cell seq to assess DE. Similar to the previous two experiments, a few genes (6 downregulated and 1 upregulated) were identified as DE across any KC subtype between CIT-fed and control flies (Fig. 5B–D, Supplementary Table T5). As predicted, there was no "pileup" of these observations on chr2R (Fig. 5E).

To formally assess concordance between the five datasets, we constructed correlation plots displaying pairwise comparisons of the $\log_2$(fold-change) values for each DE observation. To compare our bulk RNA-seq for *dSERT*^{16} vs. *dSERT*^{4} with our first scRNA-seq experiment using the same alleles, we first collapsed all cell types in the scRNA-seq into one and conducted "pseudobulk" analysis on the entire population of cells. Correlation between these two measures revealed that the bulk RNA-seq picked up many more DEGs (161) than "pseudobulk" from scRNA-seq (26) (Fig. 6A). Many genes, however, exhibited fold-change values of the same sign (up or downreg), even if p_{adj} was only significant in one dataset. Notably, several genes (*Cbp53E*, *otk*, *CG42392*, *Snp*, *RpLP2*,

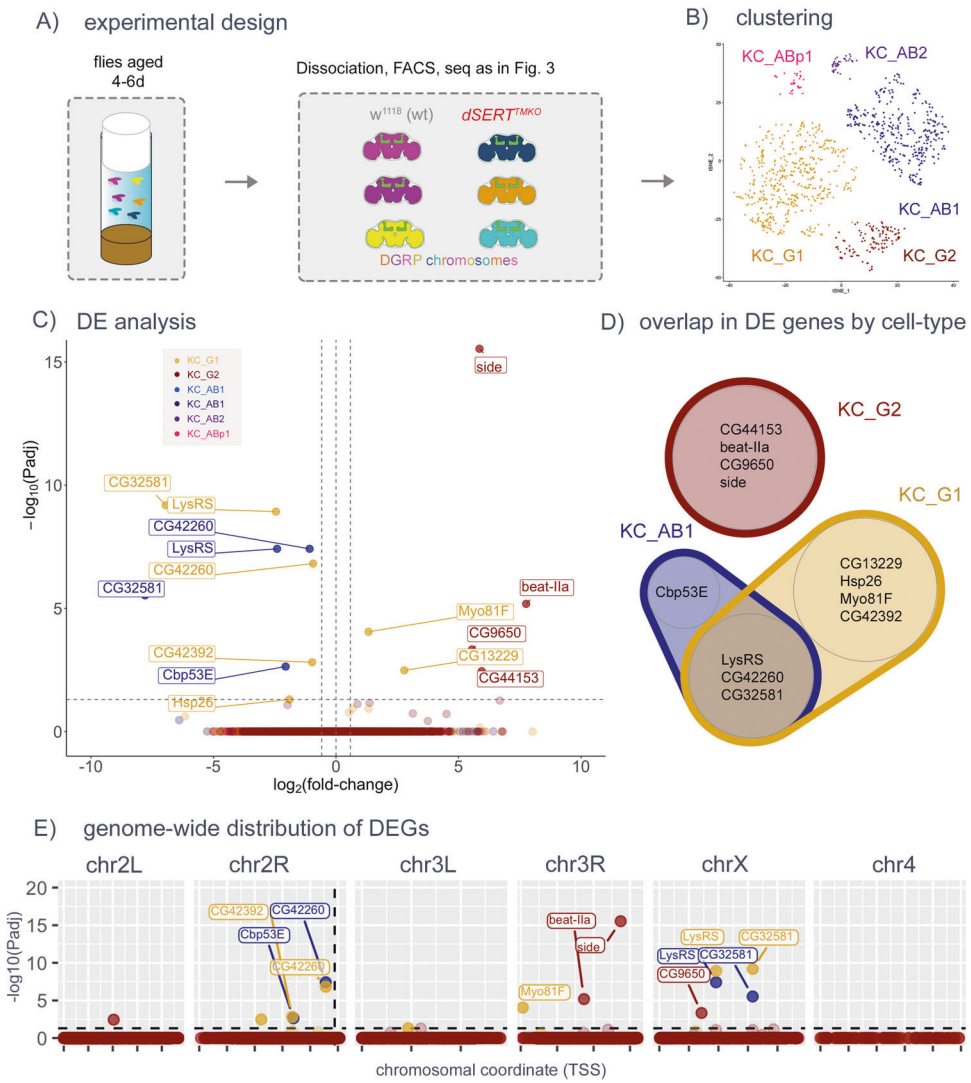

Fig. 4 scRNA-seq for d*SERT*^{TMKO} vs. controls in aged (day 4–6) flies. A Flies harboring the *dSERT*^{TMKO} or WT *dSERT* alleles (in the control line *w*^{1118}) were aged for 4–6 days and then processed for scRNA-seq as in Fig. 3. **B** t-SNE plot showing identified cell clusters color-coded by KC-type. **C** Volcano plot as in Figs. 2 and 3C from "pseudobulk" analysis (by cluster) of DEGs between mutant and control. Cell-type specific DEGs include *beat-IIa* and *side* in KC_G2, *Myo81F* in KC_G1, *Cbp53E* in KC_AB1, and *LysRS* in KC_G1 and KC_AB1, which was also DE at day 0. **D** Venn Diagram showing overlap of DEGs identified in the major cell clusters. *LysRS*, *CG42260,* and *CG32581* were identified as DE in both KC_AB1 and KC_G1. **E** DEGs plotted by chromosomal position as in Figs. 2 and 3F. Similar to Fig. 3 and in contrast to Fig. 2, observations are not concentrated on chr2R.

CG31690) were concordant between datasets, exclusive of those such as *prom* flagged as artifacts. Next, we compared the *dSERT*^{16} and *dSERT*^{TMKO} day 0 scRNA-seq datasets in a similar correlation plot but retained the cell-type specific DE conducted in the original analysis (Fig. 6B). Again, most DE observations were significant in only one dataset (smaller labels), though *CG42392* was concordant and significant in KC_G1 and KC_G2 in both datasets. Comparison of the *dSERT*^{TMKO} day 0 and day 4–6 datasets similarly revealed only two concordant changes that were significant in both datasets (Fig. 6C), *CG42392* and *LysRS* in KC_G1. Finally, a comparison of the *dSERT*^{TMKO} day 4–6 and CIT-fed day 4–6 experiments showed no concordant changes that were significant in both datasets, but many that were significant in one (Fig. 6D).

DISCUSSION

We have tested whether specific subtypes of post-synaptic cells in a defined serotonergic circuit undergo transcriptional changes in response to the inhibition of dSERT. A large number of previous reports have investigated transcriptomic changes in response to SSRI-like perturbations, but most have used peripheral samples or highly heterogenous brain tissue as input. More recently, specific subtypes of neurons have been targeted using molecular-genetic strategies employed in rodents such as RiboTag [21, 77] and untargeted scRNA-seq [14]. We have now employed similar strategies on the fly with an additional purification step—FACS sorting of GFP-labeled cells to isolate a genetically labeled neuronal subtype: the KCs of the mushroom bodies. We have also compared our DE results obtained across two independently derived, *dSERT* mutant alleles, two different age groups, and against pharmacological SERT inhibition. Our efforts here focusing on KCs have uncovered a small number of possible DEG candidates and defined several experimental pitfalls to consider in the further analysis of serotonergic signaling in the fly. Since the molecular machinery for serotonergic signaling is conserved from flies to humans we speculate that future experiments using similar

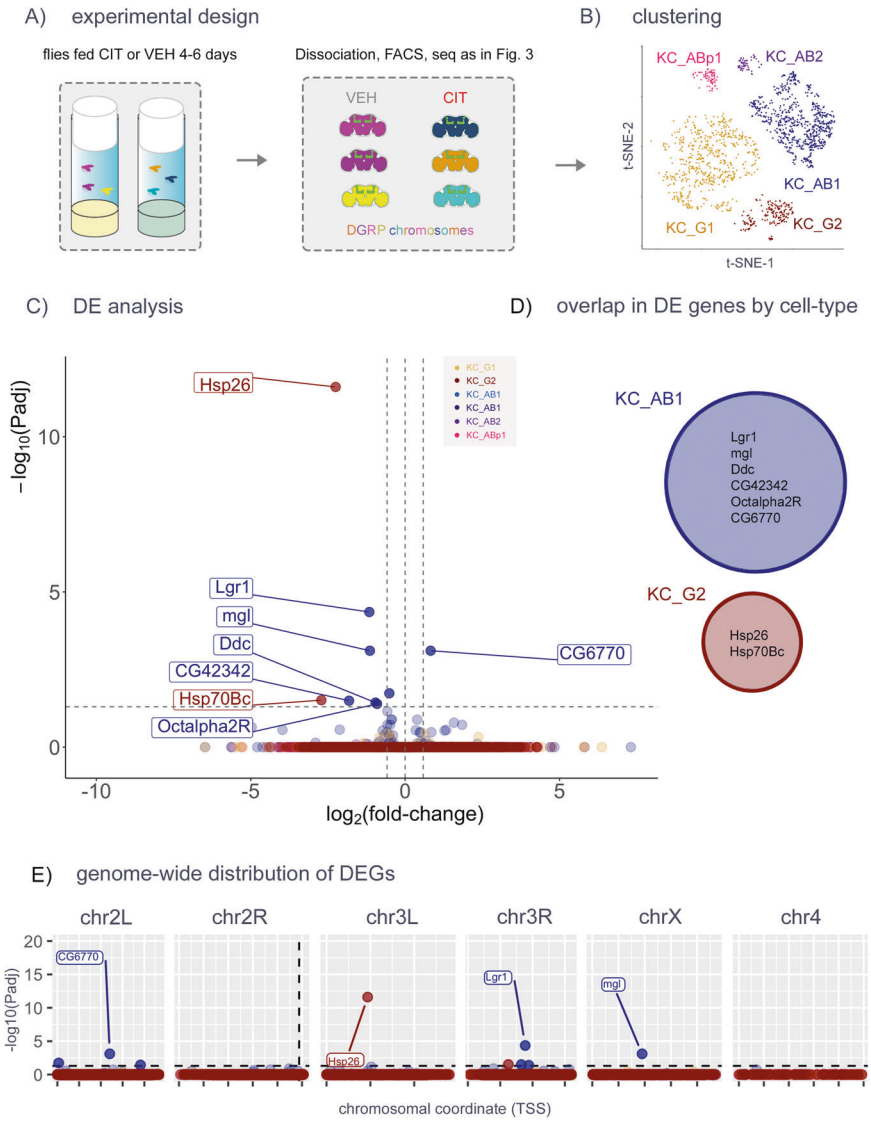

Fig. 5 scRNA-seq in aged flies treated with an SSRI. A Flies homozygous for the WT *dSERT* allele were treated with citalopram (CIT) to block SERT protein activity or vehicle alone (VEH). Each fly contained one copy of 2nd and 3rd chromosomes derived from a unique DGRP line and transgenes for marking KCs as in Figs. 2–4. **B** t-SNE plot indicating the distribution of cells by cell type. **C** Volcano plot from "pseudobulk" analysis (by cluster) of DEGs between mutant and control. Cell-type specific DEGs include *Lgr1* and *Ddc* in KC_AB1 and *Hsp26* and *Hsp70Bc* in KC_G2, none of which were identified in previous experiments. **D** Venn Diagram showing that there is no overlap of DEGs identified in the major cell clusters. **E** DEGs plotted by chromosomal position as in previous figs. Similar to Figs. 3 and 4, observations are not concentrated on chr2R.

methods may complement experiments in rodents to determine how different serotonergic circuits respond to inhibition of SERT.

Bulk RNA-seq

We initially used a high-sensitivity bulk RNA-seq method (SMART-seq) to profile changes in $dSERT^{16}$ mutant vs. $dSERT^{4}$ control flies, dissected on the day they eclosed as adults from pupae (day 0). Since we used a bulk sequencing method, reads from different KC subtypes were analyzed as a group. PCA revealed a strong separation of samples by genotype and the elimination of one set of slight outlier samples (data not shown). Standard data processing and calculation of DE revealed 98 DEGs ($p_{adj} \leq 0.05$). We note that this number is too low for gene ontology (GO) or similar analyses [78, 79] (data not shown) and that gene set enrichment analysis (GSEA) is not readily available for *Drosophila* [80]. Importantly, the number of genes we identified is comparable to the number of changes in ribosome-loaded transcripts observed in specific mouse cell types after SSRI treatment, including serotonergic neurons of the raphe nucleus [77] and S100a10 corticostriatal neurons [21], and the lower range (48–1243 DEGs) of an additional 27 brain regions recently analyzed in mice [14]. However, we also observed an enrichment of DEGs on chr2R, proximal to the *dSERT* locus, suggesting that their differential expression might be artefactual, and derived from the dysregulation of adjacent or distal DNA affected by the deletion, or perhaps genetic linkage.

scRNA-seq

Studies using bulk RNA-seq methods such as SMART-seq are limited by the heterogeneity of the cell types used for input. In addition, it is known that small differences in sample treatment, even in those processed simultaneously and in parallel, contribute significantly to noise in sequencing data. To address these concerns, we used a newly developed scRNA-seq protocol to "tag" different biological replicates with different

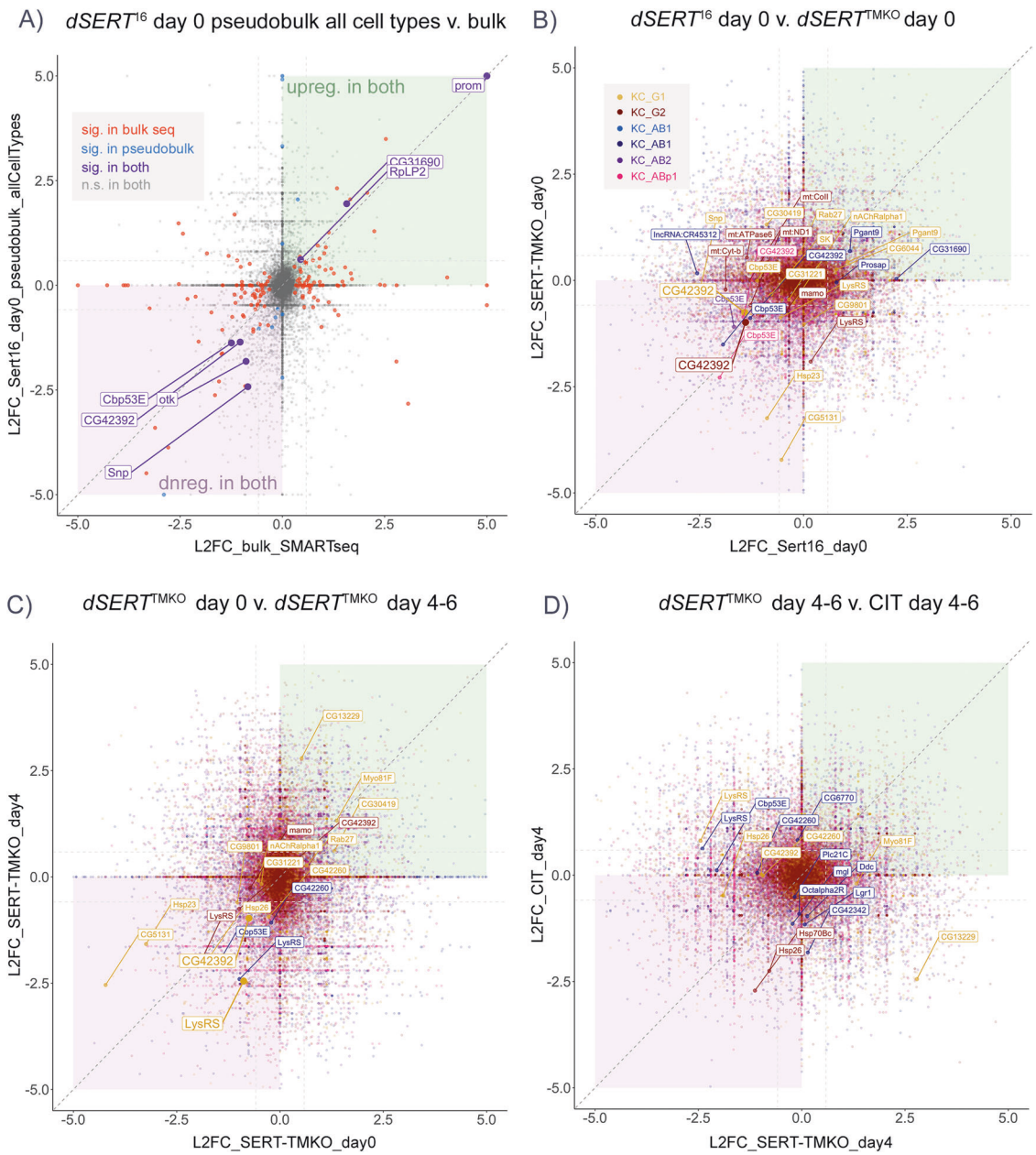

Fig. 6 Correlation of genes identified as DE between datasets. A Correlation plot showing $\log_2$(fold-change) (L2FC) for DEGs in *dSERT*^{16} versus *dSERT*^{4} at day 0, comparing bulk sequencing (Fig. 1) and the initial scRNA-seq data (Fig. 2) analyzed using "pseudobulk" to collapse all clusters into one artificial "cell-type" for comparison with the bulk dataset. Concordant genes significant in both datasets are plotted in a larger font and colored purple. Genes significant in only the bulk or scRNA-seq datasets are colored red or blue, respectively. Diagonal dark gray dashed line represents a 1:1 correlation between datasets. The lighter gray horizontal and vertical lines represent 1.5 fold-change cutoffs for genes of interest. **B** Correlation plot between *dSERT*^{16} and *dSERT*^{TMKO} day 0 scRNA-seq datasets. Genes are color-coded by KC type as in previous figures. Genes not significant in either dataset are plotted with reduced opacity. Genes significant in at least one dataset are plotted with normal opacity. While there are many genes with L2FC of the same sign in both datasets, most are only significant in one dataset (smaller labeled points). **C** Correlation plot comparing data derived from newly eclosed (day 0) vs. aged flies (day 4–6) using the *dSERT*^{TMKO}. Genes are plotted as in (**B**). *CG42392* and *LysRS* in KC_G1 were significant in both datasets (larger labels and points), with DE in the same direction (downregulated). **D** Correlation plot between aged d*SERT*^{TMKO} (d4–6) and aged flies fed citalopram (CIT). One gene (*Hsp26*) was DE in both datasets, although in a different cell type in each dataset and therefore not highlighted.

DGRP chromosomes, thus allowing them to be processed as a single sample [43]. In the first of these experiments, we again used *dSERT*^{16} mutant and *dSERT*^{4} control flies at day 0 post-eclosion. We observed an even more pronounced enrichment of DEGs on chr2R proximal to the *dSERT* locus, further suggesting that relatively small changes in genetic architecture can significantly affect the detection of transcriptomic differences.

To avoid the chromosomal effects of the *dSERT*^{16} imprecise excision allele, we generated a new mutant allele using CRISPR/Cas9 (*dSERT*^{TMKO}). In contrast to *dSERT*^{16}, the *dSERT*^{TMKO} deletion does not include DNA upstream of the start codon that may be more likely to contribute to the regulation of transcription of adjacent genes. We repeated the scRNA-seq experiment at day 0 using *dSERT*^{TMKO} and found that most of the DEGs on chr2R suspected to be artifactual in the *dSERT*^{16} dataset were absent in

the *dSERT*^{TMKO} dataset, including *prom*, an eye-specific gene 4.3 kb upstream of *dSERT*. Together, the data shown in Figs. 2 and 3 indicate that mutations in *dSERT* and other genes used in further analyses should be carefully selected to minimize the disruption of chromosomal architecture.

Interestingly, one of the few DEGs identified in the *dSERT*^{TMKO} day 0 dataset was *dpr1* in KC_ABp1, a cell-adhesion molecule that may represent an adjustment to dysregulated circuit activity in the presence of aberrant serotonergic signaling. SERT is present in developing serotonergic neurons [81], and SSRIs can cause dysregulation of circuit wiring in mammals [82–84]. Additionally, *Drosophila* serotonergic neurons are remodeled and form new synapses in development [85]. Many cells that express 5-HTRs undergo significant changes in gene expression during this time [43, 86] and are further refined by activity [87–89]. It is plausible that other factors involved in circuit formation and stabilization may be targets of homeostatic adjustments in response to altered extracellular serotonin.

Adult versus developmental effects of SERT LOF

We hypothesized that loss of dSERT activity during both development and adulthood, rather than development alone, might further alter the DE profile. To test this, we repeated the scRNA-seq protocol using flies that had been aged for 4–6 days rather than freshly eclosed (day 0). We again observed some changes across multiple cell types (i.e. *LysRS*, *CG42260*), as well as some that were cell-type specific. Among these, the cell surface recognition molecules *beat-IIa* and *side* DE in KC_G2 could, similarly to *dpr1* in KC_AB1 in the experiment with day 0 flies, represent homeostatic changes to maintain proper connectivity. However, the total number of DEGs seen in the aged flies was similar to that seen with newly eclosed flies.

To further explore the effects of dSERT inhibition in the adult, we fed WT flies the SSRI citalopram (CIT) or vehicle (VEH) for 4–6 days and repeated our scRNA-seq workflow. We uncovered a new set of DEGs, most of which were observed only in the major $KC_{\alpha/\beta}$ subtype (KC_AB1) and which did not show significant overlap with those detected using mutants. It is possible that off-target effects of CIT dominate these observations, and drug specificity may be tested in future experiments by feeding CIT to *dSERT* mutants. It is also possible that the decrease in SERT activity caused by citalopram was less pronounced than the complete block in activity caused by *dSERT*^{TMKO}, thus reducing the change in serotonergic singaling and the subsequent effects on post-synaptic cells. Alternatively, the very low number of DEGs we detect in adult flies fed citalopram, as well as the relatively small difference in the number of DEGs in day 0 versus day 4–6 *dSERT*^{TMKO} may be consistent with the idea that serotonergic signaling during development exerts more significant changes than inhibition of SERT in the adult. Further genetic methods to knock out *dSERT* during development versus in adult flies will be used to address this issue. We note that in mouse models, many effects on behavior seen with both SSRIs and mutants that perturb serotonergic signaling are primarily based on exposure during development [83, 90–95].

Cell-subtype-specific effects

Some of the DE observed in our scRNA-seq experiments appeared to be specific to particular KC types. It is possible that these differences arise from the different expression profiles of 5-HTRs, including the enrichment of 5-HT1A on $KC_{\alpha/\beta}$ and 5-HT1B on KC_{γ}. It is also possible that differences in the extent or source of serotonergic innervation of different KC subtypes contributed to these differences. Our data show that although the number of detectable changes in response to dSERT LOF is low in this system, even highly similar cell types (KC subtypes) exhibit different changes in response to the same chronic perturbation. Recent results in mice suggest a similarly heterogenous response in subtypes of hippocampal neurons [14]. We suggest that further experiments in the fly will complement studies in mammals to determine the molecular mechanisms by which serotonergic drugs exert their effects on different subsets of neurons.

Technical and experimental limitations

Across all of our single-cell RNA-seq experiments, both during development and in the adult, the total number of DEGs was lower than those identified in the initial bulk RNA-seq experiment. In contrast to the single-cell protocol, SMART-seq captures cells in a chaotropic agent that halts transcriptional dysregulation induced by cell injury and protects RNA from degradation. This difference, and/or differences in library prep methodologies between SMART-seq and *10x* 3′GEX may have led to better detection of DEGs in our bulk RNA-seq experiment. More generally, it is known that the advantages of scRNA-seq come at the cost of low sequencing depth per cell.

Several additional factors may contribute to the low number of DE genes we observed in single-cell experiments, including relatively low numbers of cells in some clusters (Supplementary Fig. S1F). Our power to detect DE was strongest in the clusters with the highest cell number (KC_AB1 and KC_G1) and more cells may be needed to detect subtle changes in gene expression in other subtypes. The stringent nature of our analyses may also have excluded some subtle or variable changes. The percentage of *p*-values that survived *Benjamini–Hochberg* multiple comparison corrections in each of our scRNA-seq "pseudobulk" analyses was between 2% and 8%. This represents a standard tradeoff in sequencing studies between the unbiased measurement of all genes in the genome at the statistical cost of multiple comparisons. Unfortunately, this also presents a significant barrier in all current studies attempting to identify less consistent or smaller changes. Finally, it is possible that the sample prep methodology should be further refined for this type of investigation. For example, in future experiments, we will consider alternative methods such as flash-freezing tissue [96, 97], which may result in a faster and cleaner sample prep with fewer artefactual changes.

In addition to a relatively small number of DEGs per experiment, comparing our datasets in correlation plots reveals relatively little overlap. This may suggest that genomic background and experimental variability have stronger effects on DE analysis between groups than the effects of dSERT LOF. The least favorable interpretation of this lack of overlap is that most of the DEGs we detected were "noise", however, the stringent statistical analysis suggests otherwise. Based on both the relatively small number of DEGs as well as the relatively limited overlap we observe across experiments, we speculate that the specific post-synaptic cells we chose to study (KCs) may not mount a large transcriptional response to changes in serotonergic signaling. Using the myriad of available drivers to label and isolate different cell types in the fly may reveal different cell types that show more robust transcriptional responses to mutation of *dSERT* or feeding SSRIs than we identified in KCs. In addition, while neuronal excitation [98, 99] and even the signaling cascades modulated by serotonin are known to be intimately linked to transcription [100], these pathways are also regulated by many other factors. Serotonergic signaling may only cause weak or microdomain-restricted changes in some pathways, and it is possible that the primary adaptive response to an increase in extracellular serotonin is post-transcriptional. Additional -omic strategies, notably ChIP-seq and ATAC-seq [101, 102], have been used with great success from similar starting samples, and provide a complementary approach to RNA-seq in future studies.

Candidate genes for further investigation

Despite the low number of observations in this study, those identified may represent a true response to the inhibition of dSERT

and changes in extracellular serotonin. If so, they are novel. These include *Cbp53E*, an ortholog of *calbindin* known to affect axon branching in *Drosophila* [103], and *pgant9*, an enzyme involved in the sugar-modification of proteins [104, 105]. While further validation will be needed, we suggest that concordance across datasets may justify further investigation of these and other DEGs. In *Drosophila*, testing the functional effects of perturbing candidate genes, rather than additional molecular methods such as RT-qPCR or in situ hybridization, maybe the most efficient path to testing their validity. The large number of mutants available on the fly as well as the low cost of generating new mutants underscore the power of this approach and its complementary use with RNA-seq studies compared to those conducted in other model systems such as rodents.

DATA AVAILABILITY

All raw data and Seurat objects generated in this study are available on GEO at accession number GSE227935. No new algorithms were developed in this work.

CODE AVAILABILITY

Code for data processing and figure creation is available upon request.

REFERENCES

1. Ren J, Isakova A, Friedmann D, Zeng J, Grutzner SM, Pun A, et al. Single-cell transcriptomes and whole-brain projections of serotonin neurons in the mouse dorsal and median raphe nuclei. Marder E, Nelson SB, Gaspar P, editors. eLife. 2019;8:e49424.
2. Charnay Y, Leger L. Brain serotonergic circuitries. Dialogues Clin Neurosci. 2010;12:471–87.
3. Belmaker RH, Agam G. Major depressive disorder. N Engl J Med. 2008;358:55–68.
4. Ravindran LN, Stein MB. The pharmacologic treatment of anxiety disorders: a review of progress. J Clin Psychiatry. 2010;71:839–54.
5. Saravanakumar A, Sadighi A, Ryu R, Akhlaghi F. Physicochemical properties, biotransformation, and transport pathways of established and newly approved medications: a systematic review of the top 200 most prescribed drugs vs. the FDA-approved drugs between 2005 and 2016. Clin Pharmacokinet 2019;58:1281–94.
6. Tanne JH. Antidepressants surpass antihypertensives as most commonly prescribed drugs in US. BMJ 2009;339:b3380.
7. Moncrieff J, Cooper RE, Stockmann T, Amendola S, Hengartner MP, Horowitz MA. The serotonin theory of depression: a systematic umbrella review of the evidence. Mol Psychiatry. 2022;1–14.
8. Kambeitz JP, Howes OD. The serotonin transporter in depression: Meta-analysis of in vivo and post mortem findings and implications for understanding and treating depression. J Affect Disord. 2015;186:358–66.
9. Hagino Y, Takamatsu Y, Yamamoto H, Iwamura T, Murphy DL, Uhl GR, et al. Effects of MDMA on extracellular dopamine and serotonin levels in mice lacking dopamine and/or serotonin transporters. Curr Neuropharmacol. 2011;9:91–5.
10. Meyer JH. Imaging the serotonin transporter during major depressive disorder and antidepressant treatment. J Psychiatry Neurosci. 2007;32:86–102.
11. Beyazyüz M, Albayrak Y, Eğilmez OB, Albayrak N, Beyazyüz E. Relationship between SSRIs and metabolic syndrome abnormalities in patients with generalized anxiety disorder: a Prospective Study. Psychiatry Investig. 2013;10:148–54.
12. Halperin D, Reber G. Influence of antidepressants on hemostasis. Dialogues Clin Neurosci. 2007;9:47–59.
13. Flechtner-Mors M, Jenkinson CP, Alt A, Adler G, Ditschuneit HH. Metabolism in adipose tissue in response to citalopram and trimipramine treatment—an in situ microdialysis study. J Psychiatr Res. 2008;42:578–86.
14. Rayan NA, Kumar V, Aow J, Rastegar N, Lim MGL, O'Toole N, et al. Integrative multi-omics landscape of fluoxetine action across 27 brain regions reveals global increase in energy metabolism and region-specific chromatin remodelling. Mol Psychiatry. 2022;27:4510–25.
15. Glover ME, McCoy CR, Shupe EA, Unroe KA, Jackson NL, Clinton SM. Perinatal exposure to the SSRI paroxetine alters the methylome landscape of the developing dentate gyrus. Eur J Neurosci. 2019;50:1843–70.
16. Calizo LH, Akanwa A, Ma X, Pan YZ, Lemos JC, Craige C, et al. Raphe serotonin neurons are not homogenous: electrophysiological, morphological and neurochemical evidence. Neuropharmacology 2011;61:524–43.
17. Okaty BW, Commons KG, Dymecki SM. Embracing diversity in the 5-HT neuronal system. Nat Rev Neurosci. 2019;20:397–424.
18. Frazer S, Prados J, Niquille M, Cadilhac C, Markopoulos F, Gomez L, et al. Transcriptomic and anatomic parcellation of 5-HT3AR expressing cortical interneuron subtypes revealed by single-cell RNA sequencing. Nat Commun. 2017;8:14219.
19. Winterer J, Lukacsovich D, Que L, Sartori AM, Luo W, Földy C. Single-cell RNA-Seq characterization of anatomically identified OLM interneurons in different transgenic mouse lines. Eur J Neurosci. 2019;50:3750–71.
20. Schmidt EF, Warner-Schmidt JL, Otopalik BG, Pickett SB, Greengard P, Heintz N. Identification of the cortical neurons that mediate antidepressant responses. Cell 2012;149:1152–63.
21. Sargin D, Chottekalapanda RU, Perit KE, Yao V, Chu D, Sparks DW, et al. Mapping the physiological and molecular markers of stress and SSRI antidepressant treatment in S100a10 corticostriatal neurons. Mol Psychiatry. 2020;25:1112–29.
22. Alekseyenko OV, Lee C, Kravitz EA. Targeted Manipulation of Serotonergic Neurotransmission Affects the Escalation of Aggression in Adult Male Drosophila melanogaster. PLoS ONE. 2010;5:e10806.
23. Monastirioti M. Biogenic amine systems in the fruit fly Drosophila melanogaster. Microsc Res Tech. 1999;45:106–21.
24. Vallés AM, White K. Serotonin-containing neurons in Drosophila melanogaster: development and distribution. J Comp Neurol. 1988;268:414–28.
25. Modi MN, Shuai Y, Turner GC. The *Drosophila* mushroom body: from architecture to algorithm in a learning circuit. Annu Rev Neurosci. 2020;43:465–84.
26. Scheunemann L, Plaçais PY, Dromard Y, Schwärzel M, Preat T. Dunce phosphodiesterase acts as a checkpoint for Drosophila long-term memory in a pair of serotonergic neurons. Neuron 2018;98:350–365.e5.
27. Coates KE, Calle-Schuler SA, Helmick LM, Knotts VL, Martik BN, Salman F, et al. The wiring logic of an identified serotonergic neuron that spans sensory networks. J Neurosci. 2020;40:6309–27.
28. Coates KE, Majot AT, Zhang X, Michael CT, Spitzer SL, Gaudry Q, et al. Identified serotonergic modulatory neurons have heterogeneous synaptic connectivity within the olfactory system of Drosophila. J Neurosci. 2017;37:7318–31.
29. Dacks AM, Christensen TA, Hildebrand JG. Phylogeny of a serotonin-immunoreactive neuron in the primary olfactory center of the insect brain. J Comp Neurol. 2006;498:727–46.
30. Suzuki Y, Schenk JE, Tan H, Gaudry Q. A population of interneurons signals changes in the basal concentration of serotonin and mediates gain control in the drosophila antennal lobe. Curr Biol. 2020;30:1110–1118.e4.
31. Zhang X, Gaudry Q Functional integration of a serotonergic neuron in the Drosophila antennal lobe. eLife. 2016:16836.
32. Tanaka NK, Tanimoto H, Ito K. Neuronal assemblies of the Drosophila mushroom body. J Comp Neurol. 2008;508:711–55.
33. Shih MFM, Davis FP, Henry GL, Dubnau J. Nuclear transcriptomes of the seven neuronal cell types that constitute the Drosophila mushroom bodies. G3 Bethesda MD. 2019;9:81–94.
34. Aso Y, Ray RP, Long X, Bushey D, Cichewicz K, Ngo TT, et al. Nitric oxide acts as a cotransmitter in a subset of dopaminergic neurons to diversify memory dynamics. VijayRaghavan K, Ramaswami M, Strauss RH, editors. eLife. 2019;8:e49257.
35. Majeed ZR, Abdeljaber E, Soveland R, Cornwell K, Bankemper A, Koch F, et al. Modulatory action by the serotonergic system: behavior and neurophysiology in *Drosophila melanogaster*. Neural Plast. 2016;2016:7291438.
36. Ries AS, Hermanns T, Poeck B, Strauss R. Serotonin modulates a depression-like state in Drosophila responsive to lithium treatment. Nat Commun. 2017;8:15738.
37. Yuan Q, Joiner WJ, Sehgal A. A sleep-promoting role for the Drosophila Serotonin Receptor 1A. Curr Biol. 2006;16:1051–62.
38. Gratz SJ, Ukken FP, Rubinstein CD, Thiede G, Donohue LK, Cummings AM, et al. Highly specific and efficient CRISPR/Cas9-catalyzed homology-directed repair in Drosophila. Genetics 2014;196:961–71.
39. Moreno-Mateos MA, Vejnar CE, Beaudoin JD, Fernandez JP, Mis EK, Khokha MK, et al. CRISPRscan: designing highly efficient sgRNAs for CRISPR-Cas9 targeting in vivo. Nat Methods. 2015;12:982–8.
40. Doench JG, Fusi N, Sullender M, Hegde M, Vaimberg EW, Donovan KF, et al. Optimized sgRNA design to maximize activity and minimize off-target effects of CRISPR-Cas9. Nat Biotechnol. 2016;34:184–91.
41. Gratz SJ, Rubinstein CD, Harrison MM, Wildonger J, O'Connor-Giles KM. CRISPR-Cas9 genome editing in Drosophila. Ed Frederick M Ausubel AL. Curr Protoc Mol Biol 2015;111:31.2.1–31.2.20.
42. Siegal ML, Hartl DL. Transgene coplacement and high efficiency site-specific recombination with the Cre/Loxp system in Drosophila. Genetics 1996;144:715–26.
43. Kurmangaliyev YZ, Yoo J, Valdes-Aleman J, Sanfilippo P, Zipursky SL. Transcriptional programs of circuit assembly in the Drosophila visual system. Neuron 2020;108:1045–1057.e6.

44. Tan L, Zhang KX, Pecot MY, Nagarkar-Jaiswal S, Lee PT, Takemura SY, et al. Ig superfamily ligand and receptor pairs expressed in synaptic partners in Drosophila. Cell 2015;163:1756–69.
45. Picelli S, Björklund ÅK, Faridani OR, Sagasser S, Winberg G, Sandberg R. Smart-seq2 for sensitive full-length transcriptome profiling in single cells. Nat Methods. 2013;10:1096–8.
46. Picelli S, Faridani OR, Björklund ÅK, Winberg G, Sagasser S, Sandberg R. Full-length RNA-seq from single cells using Smart-seq2. Nat Protoc. 2014;9:171–81.
47. Dobin A, Davis CA, Schlesinger F, Drenkow J, Zaleski C, Jha S, et al. STAR: ultrafast universal RNA-seq aligner. Bioinforma Oxf Engl. 2013;29:15–21.
48. Love MI, Huber W, Anders S. Moderated estimation of fold change and dispersion for RNA-seq data with DESeq2. Genome Biol. 2014;15:550.
49. Kang HM, Subramaniam M, Targ S, Nguyen M, Maliskova L, McCarthy E, et al. Multiplexed droplet single-cell RNA-sequencing using natural genetic variation. Nat Biotechnol. 2018;36:89–94.
50. Huang W, Massouras A, Inoue Y, Peiffer J, Ràmia M, Tarone AM, et al. Natural variation in genome architecture among 205 *Drosophila melanogaster* Genetic Reference Panel lines. Genome Res. 2014;24:1193–208.
51. Zhao H, Sun Z, Wang J, Huang H, Kocher JP, Wang L. CrossMap: a versatile tool for coordinate conversion between genome assemblies. Bioinforma Oxf Engl. 2014;30:1006–7.
52. Danecek P, Auton A, Abecasis G, Albers CA, Banks E, DePristo MA, et al. The variant call format and VCFtools. Bioinforma Oxf Engl. 2011;27:2156–8.
53. Li H. A statistical framework for SNP calling, mutation discovery, association mapping and population genetical parameter estimation from sequencing data. Bioinformatics 2011;27:2987–93.
54. Stuart T, Butler A, Hoffman P, Hafemeister C, Papalexi E, Mauck WM, et al. Comprehensive integration of single-cell data. Cell 2019;177:1888–1902.e21.
55. Hao Y, Hao S, Andersen-Nissen E, Mauck WM, Zheng S, Butler A, et al. Integrated analysis of multimodal single-cell data. Cell 2021;184:3573–3587.e29.
56. Squair JW, Gautier M, Kathe C, Anderson MA, James ND, Hutson TH, et al. Confronting false discoveries in single-cell differential expression. Nat Commun. 2021;12(Sep):5692.
57. Wickham, H. ggplot2: elegant graphics for data analysis. New York: Springer-Verlag; 2016.
58. Wickham H, Averick M, Bryan J, Chang W, McGowan LD, François R, et al. Welcome to the Tidyverse. J Open Source Softw. 2019;4(Nov):1686.
59. Slowikowski K. ggrepel: automatically position non-overlapping text labels with 'ggplot2'. R package version 0.9.3, https://github.com/slowkow/ggrepel. 2023.
60. Pedersen TL. patchwork. https://github.com/thomasp85/patchwork. 2022.
61. Pérez-Silva JG, Araujo-Voces M, Quesada V. nVenn: generalized, quasi-proportional Venn and Euler diagrams. Bioinformatics 2018;34(Jul):2322–4.
62. Squair J, Yang ATY. neurorestore. https://github.com/neurorestore/Libra. 2021.
63. Robinson MD, McCarthy DJ, Smyth GK. edgeR: a Bioconductor package for differential expression analysis of digital gene expression data. Bioinformatics 2010;26:139–40.
64. McCarthy DJ, Chen Y, Smyth GK. Differential expression analysis of multifactor RNA-Seq experiments with respect to biological variation. Nucleic Acids Res. 2012;40:4288–97.
65. Ritchie ME, Phipson B, Wu D, Hu Y, Law CW, Shi W, et al. limma powers differential expression analyses for RNA-sequencing and microarray studies. Nucleic Acids Res. 2015;43:e47.
66. Butler A, Hoffman P, Smibert P, Papalexi E, Satija R. Integrating single-cell transcriptomic data across different conditions, technologies, and species. Nat Biotechnol. 2018;36:411–20.
67. Knapp EM, Kaiser A, Arnold RC, Sampson MM, Ruppert M, Xu L, et al. Mutation of the *Drosophila melanogaster* serotonin transporter dSERT impacts sleep, courtship, and feeding behaviors. PLoS Genet. 2022;18:e1010289.
68. Zars T, Fischer M, Schulz R, Heisenberg M. Localization of a short-term memory in Drosophila. Science 2000;288:672–5.
69. Aso Y, Grübel K, Busch S, Friedrich AB, Siwanowicz I, Tanimoto H. The mushroom body of Adult *Drosophila* characterized by GAL4 drivers. J Neurogenet. 2009;23:156–72.
70. Yang L, Li R, Kaneko T, Takle K, Morikawa RK, Essex L, et al. Trim9 regulates activity-dependent fine-scale topography in Drosophila. Curr Biol. 2014;24:1024–30.
71. Zhao G, Oztan A, Ye Y, Schwarz TL. Kinetochore proteins have a post-mitotic function in neurodevelopment. Dev Cell. 2019;48:873–882.e4.
72. Ganguly A, Qi C, Bajaj J, Lee D. Serotonin receptor 5-HT7 in Drosophila mushroom body neurons mediates larval appetitive olfactory learning. Sci Rep. 2020;10:21267.
73. Truman JW, Price J, Miyares RL, Lee T. Metamorphosis of memory circuits in Drosophila reveal a strategy for evolving a larval brain. eLife 2023;12:e80594.
74. Kunz T, Kraft KF, Technau GM, Urbach R. Origin of Drosophila mushroom body neuroblasts and generation of divergent embryonic lineages. Development 2012;139:2510–22.
75. Lee K, Doe CQ. A locomotor neural circuit persists and functions similarly in larvae and adult Drosophila. eLife 2021;10:e69767.
76. Yaniv SP, Schuldiner O. A fly's view of neuronal remodeling. Wiley Interdiscip Rev Dev Biol. 2016;5:618–35.
77. Lesiak AJ, Coffey K, Cohen JH, Liang KJ, Chavkin C, Neumaier JF. Sequencing the serotonergic neuron translatome reveals a new role for Fkbp5 in stress. Mol Psychiatry. 2020;26:1–12.
78. Chen EY, Tan CM, Kou Y, Duan Q, Wang Z, Meirelles GV, et al. Enrichr: interactive and collaborative HTML5 gene list enrichment analysis tool. BMC Bioinforma. 2013;14:128.
79. Kuleshov MV, Jones MR, Rouillard AD, Fernandez NF, Duan Q, Wang Z, et al. Enrichr: a comprehensive gene set enrichment analysis web server 2016 update. Nucleic Acids Res. 2016;44:W90–7.
80. Cheng J, Hsu LF, Juan YH, Liu HP, Lin WY. Pathway-targeting gene matrix for Drosophila gene set enrichment analysis. PLoS ONE. 2021;16:e0259201.
81. Ivgy-May N, Tamir H, Gershon M. Synaptic properties of serotonergic growth cones in developing rat brain. J Neurosci. 1994;14:1011–29.
82. Van der Knaap N, Wiedermann D, Schubert D, Hoehn M, Homberg JR. Perinatal SSRI exposure affects brain functional activity associated with whisker stimulation in adolescent and adult rats. Sci Rep. 2021;11:1680.
83. Soiza-Reilly M, Meye FJ, Olusakin J, Telley L, Petit E, Chen X, et al. Correction: SSRIs target prefrontal to raphe circuits during development modulating synaptic connectivity and emotional behavior. Mol Psychiatry. 2019;24:773–773.
84. Simpson KL, Weaver KJ, de Villers-Sidani E, Lu JYF, Cai Z, Pang Y, et al. Perinatal antidepressant exposure alters cortical network function in rodents. Proc Natl Acad Sci USA. 2011;108:18465–70.
85. Roy B, Singh AP, Shetty C, Chaudhary V, North A, Landgraf M, et al. Metamorphosis of an identified serotonergic neuron in the Drosophila olfactory system. Neural Dev. 2007;2:20.
86. Özel MN, Simon F, Jafari S, Holguera I, Chen YC, Benhra N, et al. Neuronal diversity and convergence in a visual system developmental atlas. Nature 2021;589:88–95.
87. Sanes JR, Zipursky SL. Synaptic specificity, recognition molecules, and assembly of neural circuits. Cell 2020;181:536–56.
88. Chen Y, Akin O, Nern A, Tsui CYK, Pecot MY, Zipursky SL. Cell-type specific labeling of synapses in vivo through synaptic tagging with recombination (STaR). Neuron 2014;81:280–93.
89. Akin O, Bajar BT, Keles MF, Frye MA, Zipursky SL. Cell-type-specific patterned stimulus-independent neuronal activity in the Drosophila visual system during synapse formation. Neuron 2019;101:894–904.e5.
90. Zhang ZW. Serotonin induces tonic firing in layer V pyramidal neurons of rat prefrontal cortex during postnatal development. J Neurosci. 2003;23:3373–84.
91. Sodhi MSK, Sanders-Bush E. In: International review of neurobiology: Disorders of Synaptic Plasticity and Schizophrenia, vol. 59 (ed Smythies, J.) Serotonin and brain development (Academic Press, New York, 2004).
92. Ansorge MS, Morelli E, Gingrich JA. Inhibition of serotonin but not norepinephrine transport during development produces delayed, persistent perturbations of emotional behaviors in mice. J Neurosci. 2008;28:199–207.
93. Unroe KA, Maltman JL, Shupe EA, Clinton SM. Disrupted serotonin system development via early life antidepressant exposure impairs maternal care and increases serotonin receptor expression in adult female offspring. Dev Psychobiol. 2022;64:e22292.
94. Rebello TJ, Yu Q, Goodfellow NM, Cagliostro MKC, Teissier A, Morelli E, et al. Postnatal day 2 to 11 constitutes a 5-HT-sensitive period impacting adult mPFC function. J Neurosci. 2014;34:12379–93.
95. Teissier A, Soiza-Reilly M, Gaspar P. Refining the role of 5-HT in postnatal development of brain circuits. Front Cell Neurosci. 2017;11:139.
96. Ma J, Weake VM. Affinity-based isolation of tagged nuclei from Drosophila tissues for gene expression analysis. J Vis Exp JoVE. 2014;85:51418.
97. Escobedo SE, Stanhope SC, Dong Z, Weake VM. Aging and light stress result in overlapping and unique gene expression changes in photoreceptors. Genes 2022;13:264.
98. Pan Y, He X, Li C, Li Y, Li W, Zhang H, et al. Neuronal activity recruits the CRTC1/CREB axis to drive transcription-dependent autophagy for maintaining late-phase LTD. Cell Rep. 2021;36:109398.
99. Tyssowski KM, Gray JM. The neuronal stimulation–transcription coupling map. Curr Opin Neurobiol. 2019;59:87–94.
100. Millan MJ, Marin P, Bockaert J, Mannoury, la Cour C. Signaling at G-protein-coupled serotonin receptors: recent advances and future research directions. Trends Pharm Sci. 2008;29:454–64.

101. Jain S, Lin Y, Kurmangaliyev YZ, Valdes-Aleman J, LoCascio SA, Mirshahidi P, et al. A global timing mechanism regulates cell-type-specific wiring programmes. Nature 2022;603:112–8.
102. Jauregui-Lozano J, Bakhle K, Weake VM. In vivo tissue-specific chromatin profiling in *Drosophila melanogaster* using GFP-tagged nuclei. Genetics 2021;218:iyab079.
103. Hagel KR, Beriont J, Tessier CR. Drosophila Cbp53E regulates axon growth at the neuromuscular junction. PLoS ONE. 2015;10:e0132636.
104. Ji S, Samara NL, Revoredo L, Zhang L, Tran DT, Muirhead K, et al. A molecular switch orchestrates enzyme specificity and secretory granule morphology. Nat Commun. 2018;9:3508.
105. May C, Ji S, Syed ZA, Revoredo L, Daniel EJP, Gerken TA, et al. Differential splicing of the lectin domain of an O-glycosyltransferase modulates both peptide and glycopeptide preferences. J Biol Chem. 2020;295:12525–36.

ACKNOWLEDGEMENTS

The authors wish to thank Yerbol Kurmangaliev for his thoughtful advice and for helping to demultiplex and integrate scRNA-seq data. We thank former Krantz Lab graduate student Maureen Sampson, and the Zipursky Lab at UCLA for help designing experiments. We thank Rebecca Arnold for helping to dissect flies in our initial experiments. Funding for this work included R01 MH107390 (DEK), R01 MH114017 (DEK), and a seed grant from the UCLA Depression Grand Challenge (DEK). The funders had no role in study design, data collection, and analysis, the decision to publish, or the preparation of the manuscript.

AUTHOR CONTRIBUTIONS

SLB and DEK conceived and designed all experiments. SLB performed all experiments. SLB performed the final computational analysis and generated figures. SLB and DEK wrote the manuscript.

COMPETING INTERESTS

The authors declare no competing interests.

ADDITIONAL INFORMATION

Supplementary information The online version contains supplementary material available at https://doi.org/10.1038/s41398-023-02521-3.

Correspondence and requests for materials should be addressed to David E. Krantz.

Reprints and permission information is available at http://www.nature.com/reprints

Publisher's note Springer Nature remains neutral with regard to jurisdictional claims in published maps and institutional affiliations.